



Analysis of Small-Field Dosimetry with Various Detectors

So-Yeon Park, Byeong Geol Choi, Dong Myung Lee, Na Young Jang

Department of Radiation Oncology, Veterans Health Service Medical Center, Seoul, Korea

Received 30 November 2018

Revised 14 December 2018

Accepted 14 December 2018

Corresponding author

Na Young Jang

(mumuki79@gmail.com)

Tel: 82-2-2225-4647

Fax: 82-2-2225-4640

We evaluated the performance of various detectors for small-field dosimetry with field sizes defined by a high-definition (HD) multileaf collimator (MLC) system. For small-field dosimetry, diodes referred to as “RAZOR detectors,” MOSFET detectors, and Gafchromic EBT3 films were used in this study. For field sizes less than 1×1 cm², percent depth doses (PDDs) and lateral profiles were measured by diodes, MOSFET detectors, and films, and absolute dosimetry measurements were conducted with MOSFET detectors. For comparison purposes, the same measurements were carried out with a field size of 10×10 cm². The dose distributions were calculated by the treatment planning system Eclipse. A comparison of the measurements with calculations yielded the percentage differences. With field sizes less than 1×1 cm², it was shown that most of the percentage difference values were within 5% for 6-MV and 15-MV photon beams with the use of diodes. The measured lateral profiles were well matched with those calculated by Eclipse as the field sizes increased. Except for the depths of 0.5 cm and 20 cm, there was agreement in terms of the absolute dosimetry within 10% when MOSFET detectors were used. There was good agreement between the calculations and measurements conducted using diodes and EBT films. Both diode detectors and EBT3 films were found to be appropriate options for relative measurements of PDDs and for lateral profiles.

Keywords: Small-field dosimetry, Diode, MOSFET detector, Gafchromic EBT3 film

Introduction

Following the advances in radiotherapy techniques, stereotactic radiosurgery (SRS), stereotactic body radiation therapy (SBRT), intensity modulated radiation therapy (IMRT), and volumetric modulated arc therapy (VMAT) are broadly used as techniques with advantages in maximizing the probability of local control and minimizing the incidence of normal tissue complications.¹⁻³⁾ These radiotherapy techniques use small fields with sizes less than 3×3 cm² to generate the optimal fluences that can deliver the prescription doses to target, while sparing the surrounding normal tissues.^{4,5)} With the developments of the high-definition (HD) multi-leaf collimator (MLC) system and

m3 high-resolution micro-MLC system (BrainLAB AG, Feldkirchen, Germany), the minimum beamlet sizes less than 0.30×0.30 cm² can be used. Thus, the use of small field sizes is becoming increasingly important in radiotherapy and there is increased interest in the small-field dosimetry of photon beams.⁶⁾

Small-field dosimetry in the subcentimeter range used in modern radiotherapy techniques is challenging owing to several uncertainties, including steep-dose gradients, detector sizes, lack of charged particle equilibrium, and the partial occlusion of radiation sources.⁷⁾ Furthermore, the volume averaging effect and perturbation of dosimetric detectors are well-known issues for small-field dosimetry owing to a) high atomic number materials and b) the finite

size of the active volume of the detectors.⁷⁾ Among several detectors, diode and diamond detectors have been recommended for small-field dosimetry because they have small active volumes.^{8,9)} Several studies have conducted small-field dosimetry measurements with these detectors. Accordingly, it has been demonstrated that the measured results from these detectors agreed with calculations using Monte Carlo simulations.^{10,11)} Godson et al. have reported that unshielded diodes were optimal for the measurement of photon beams in small fields, showing that deviations between measurements and calculations were less than 2%.⁷⁾ In addition to these detectors, a metal oxide semiconductor field effect transistor (MOSFET) detector has been extensively used for *in vivo* dosimetry, as well as for small-field dosimetry.¹²⁾ MOSFET detectors have been evaluated for use in small fields. Accordingly, it has been demonstrated that considerable agreements were observed among the central axis depth-dose curves obtained with MOSFET detectors.¹²⁾ To perform the 2D measurements in small fields, films were found to be an appropriate option with high-resolution and low-energy dependence advantages.¹³⁾ A number of studies have assessed the measured profiles compared to the calculated profiles, thus eliciting good agreements between them.¹³⁻¹⁵⁾

In this study, we evaluated the performance of various detectors for small-field dosimetry when field sizes were defined by HD MLC systems with the smallest widths of 0.25 cm. For field sizes smaller than $1 \times 1 \text{ cm}^2$, percent depth doses (PDDs) and lateral profiles were measured by diodes, MOSFET detectors, and films, while absolute dosimetry studies were conducted with MOSFET detectors. For comparison purposes, the same measurements were carried out with field sizes equal to $10 \times 10 \text{ cm}^2$.

Materials and Methods

1. Various detectors and calibrations

For small-field dosimetry, diodes, MOSFET detectors, and films, were used in this study. The diode, referred to as "RAZOR detector" (IBA dosimetry GmbH, Schwarzenbruck, Germany), has an active volume of 0.6 mm in diameter and 20 μm in height. It is made of an n-type implant

in p-type silicon substrate and operates in a photovoltaic mode with no bias voltage. When the detector was exposed by a radiation, electron-hole pairs were generated in silicon. Electrons were spread by the built-in electric field of the depleted region, and the electrons generated inside the depleted region gave rise to the signal. The diode detectors were calibrated by the manufacturing company according to its own calibration protocol.

A mobile MOSFET system (Best Medical Canada, Ottawa, Canada) in conjunction with a set of high-sensitivity microMOSFETs (TN-1002RDM) has a sensitive detector dimension of $0.1 \times 0.1 \text{ cm}^2$, and a layer thickness of 50 μm . For small-field dosimetry, the MOSFET detectors were positioned with their smallest dimension aligned along the beam axis. Before measurements, the MOSFET detectors were fully characterized and calibrated with the utilization of a linear accelerator.

For 2D measurements, Gafchromic EBT3 films (Ashland Inc., Covington, NJ, USA) were used that consisted of water-equivalent materials. The active layer which was related to the absorbed doses was 30 μm , and was inserted between matte polyester (thickness of 125 μm) for protection. EBT3 films were calibrated by means of a film set exposed to various doses ranging from 0 Gy to 40 Gy. A calibration curve was generated with the use of a dual-channel method which considers red and blue corrections. The films were scanned 24 h after irradiation using a flatbed scanner (Epson 10000XL, Epson Canada Ltd, Toronto, Canada) and then separated into red, green, and blue (RGB) channels at 150 dpi.

2. Analyses of PDDs and lateral profiles

For measurements, a TrueBeam STx™ linear accelerator (Varian Medical System, Palo Alto, CA, USA) was used which comprised a HD MLC system with MLC widths equal to 0.25 cm and 0.50 cm. The photon beam energies used in this study were 6 MV and 15 MV. The source-to-surface distance (SSD) was 100 cm. Field sizes were defined with the HD MLC, and were $1 \times 1 \text{ cm}^2$, $0.75 \times 0.75 \text{ cm}^2$, $0.50 \times 0.50 \text{ cm}^2$, and $0.25 \times 0.25 \text{ cm}^2$. For each field size, PDDs were acquired at various depths of 0.5 cm, 5 cm, 10 cm, and 20 cm, at the depth of maximum dose (D_{max}), with the use of diodes and MOSFET detectors. For comparison pur-

poses, a reference field size of $10 \times 10 \text{ cm}^2$ was used, and the same measurements were then obtained. For the lateral profiles, EBT3 films were inserted into solid water phantoms (Standard Grade Solid Water, Gammex, Middleton, WI, USA) at the depths of 0.5 cm, 5 cm, 10 cm, 20 cm and D_{\max} . The field sizes were $1 \times 1 \text{ cm}^2$, $0.75 \times 0.75 \text{ cm}^2$, $0.50 \times 0.50 \text{ cm}^2$, and $0.25 \times 0.25 \text{ cm}^2$. After 24 h of irradiation, EBT3 films were scanned and validated, similar to the film calibration protocol.

To calculate dose distributions, we used the commercial treatment planning system, EclipseTM (Varian Medical System, Palo Alto, CA, USA). A virtual water phantom with a volume of $40 \times 40 \times 40 \text{ cm}^3$ was generated in Eclipse. The dose distributions were calculated with the use of the anisotropic analytic algorithm (AAA, Version 10, Varian Medical System, Palo Alto, CA, USA) with a calculation grid with a size of 1 mm which was used for small fields. By comparing the measured PDDs with the calculated PDDs, the percentage difference (%diff) was calculated as follows,

$$\%diff = \frac{\text{Measurement} - \text{Calculation}}{\text{Calculation}} \times 100 \quad (1)$$

For lateral profiles, the calculated dose distributions were exported from Eclipse and then compared with the measured dose distributions.

3. Analyses of absolute doses

For absolute dosimetry, the MOSFET detectors were positioned above a 10 cm solid water phantom in order to provide a considerable backscattered dose, and a 1 cm bolus was placed on the MOSFET detectors to reduce the air-gap effect. We delivered 100 cGy to D_{\max} with a field size of $10 \times 10 \text{ cm}^2$ for the 6 MV and 15 MV photon beams. Absolute doses were acquired for the MLC-defined field sizes of $1 \times 1 \text{ cm}^2$, $0.75 \times 0.75 \text{ cm}^2$, $0.50 \times 0.50 \text{ cm}^2$, and $0.25 \times 0.25 \text{ cm}^2$, at depths of 0.5 cm, 5 cm, 10 cm, 20 cm, and at D_{\max} . For comparison purposes, a reference field size equal to $10 \times 10 \text{ cm}^2$ was used and the same measurements were then obtained.

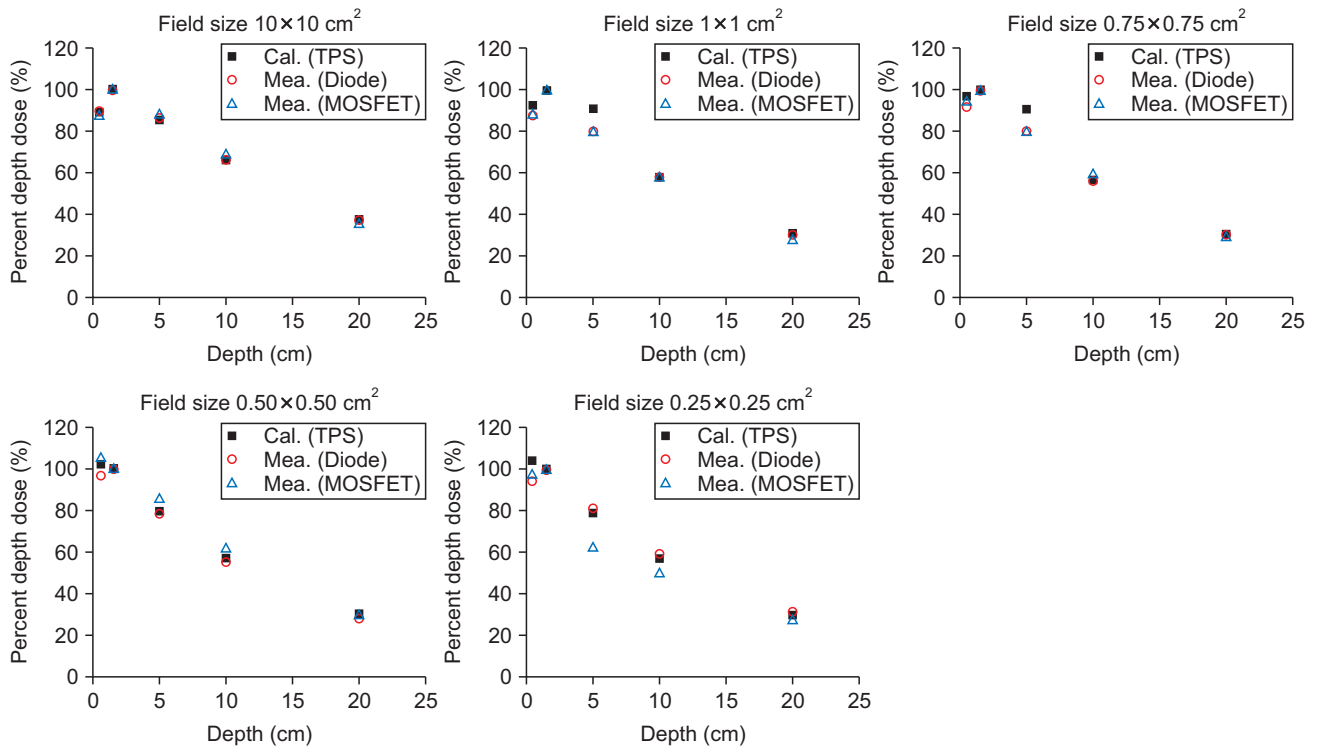


Fig. 1. Calculated and measured percent depth doses (PDDs) at various depths equal to 0.5 cm, 5 cm, 10 cm, 20 cm, and at the depth of the maximum dose (D_{\max}) for the 6 MV photon beam, and for the field sizes of $10 \times 10 \text{ cm}^2$, $1 \times 1 \text{ cm}^2$, $0.75 \times 0.75 \text{ cm}^2$, $0.50 \times 0.50 \text{ cm}^2$, and $0.25 \times 0.25 \text{ cm}^2$. The value of D_{\max} for 6 MV is 1.5 cm. TPS stands for the calculated PDDs using the Eclipse, while Diode and MOSFET stand for measured PDDs using diode and MOSFET detectors, respectively.

By comparing the measured doses with the calculated doses, the percentage difference (%diff) was calculated using equation (1).

Results

1. Analyses of PDDs and lateral profiles

Fig. 1 and 2 show calculated and measured PDDs at various depths for small fields, and a reference field for the 6 MV and 15 MV photon beams, respectively. The values of percentage differences between the calculated and measured PDDs for the 6 MV and 15 MV photon beams are also shown in Table 1. For a field size of 10×10 cm², excellent agreements between calculations and measurements were observed with the 6 MV photon beam, showing that the maximum percentage differences were 1.6% at a depth of 10 cm and -4.7% at a depth of 20 cm for diode and MOSFET detectors, respectively. Conversely, the maximum percentage differences for the 15 MV photon beam were -8.8%

and -13.0% at a depth of 0.5 cm for the diode and MOSFET detectors, respectively.

As the field sizes became smaller (less than 1×1 cm²), and percentage differences between the measurements and the calculations increased for both photon energies. With a field size of 0.25×0.25 cm², it was shown that the maximum percentage differences for the 6 MV photon beam were -9.2% at a depth of 0.5 cm, and -21.6% at a depth of 10 cm for diode and MOSFET detectors, respectively. Conversely, the maximum percentage differences for the 15 MV photon beam were -20.6% at a depth of 0.5 cm, and 22.5% at a depth of 20 cm for diode and MOSFET detectors, respectively. Overall, the percentage differences between the calculated PDDs and diode-measured PDDs were smaller than those between the calculated PDDs and MOSFET-measured PDDs.

Fig. 3 and 4 show the calculated and measured lateral profiles at various depths for small fields and reference fields for 6 MV and 15 MV photon beams, respectively. As field sizes decreased, the measured lateral profiles were not

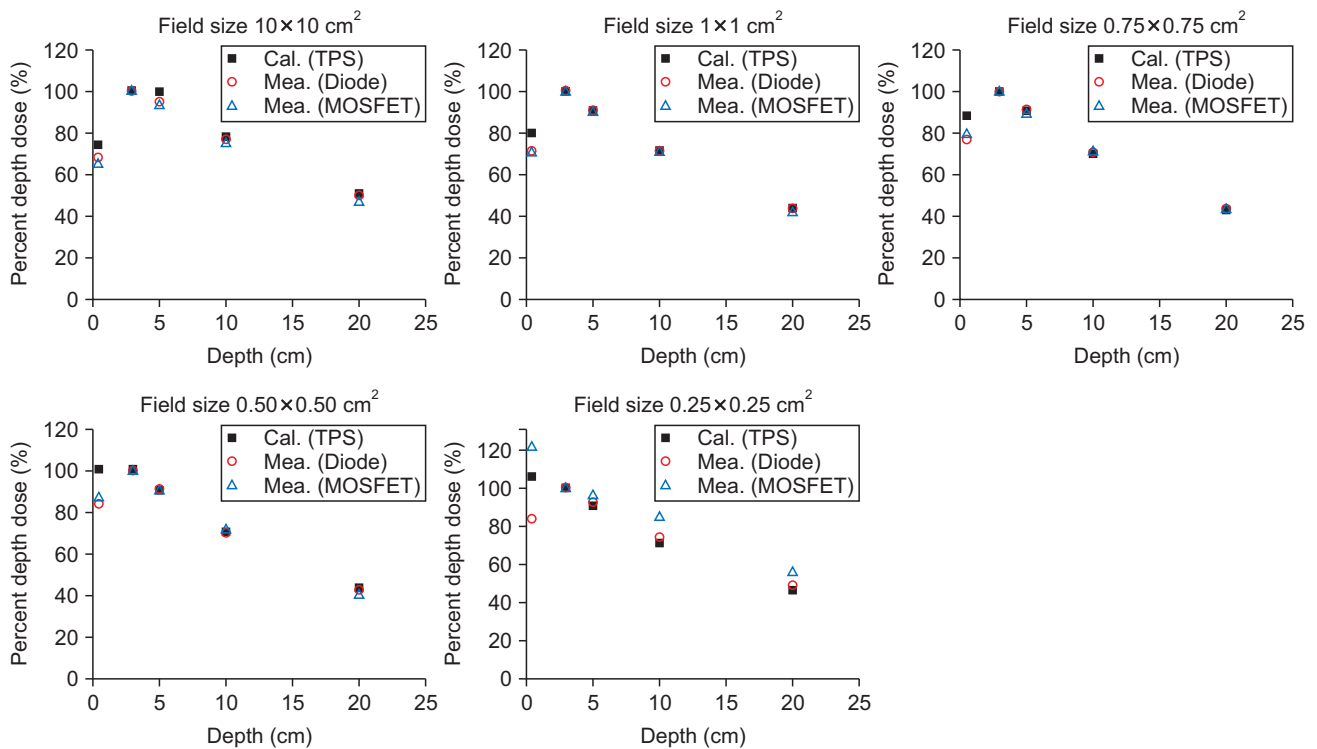


Fig. 2. Calculated and measured percent depth doses (PDDs) at various depths of 0.5 cm, 5 cm, 10 cm, 20 cm, and at the depth of the maximum dose (D_{max}) for 15 MV photon beams for the field sizes of 10×10 cm², 1×1 cm², 0.75×0.75 cm², 0.50×0.50 cm², and 0.25×0.25 cm². The value of D_{max} for 15 MV is 3 cm. TPS stands for the calculated PDDs using Eclipse while Diode and MOSFET stand for measured PDDs using diode and MOSFET detector, respectively.

Table 1. Percent differences between calculated percent depth doses (PDDs) and measured PDDs for the 6 MV and 15 MV photon beams at various depths equal to 0.5 cm, 5 cm, 10 cm, and 20 cm, and at the depth of the maximum dose (D_{max}) for the field sizes of $10 \times 10 \text{ cm}^2$, $1 \times 1 \text{ cm}^2$, $0.75 \times 0.75 \text{ cm}^2$, $0.50 \times 0.50 \text{ cm}^2$, and $0.25 \times 0.25 \text{ cm}^2$. The D_{max} values for the photon beams of 6 MV and 15 MV are respectively equal to 1.5 cm and 3 cm.

Depth (cm)	Field size										
	$10 \times 10 \text{ cm}^2$		$1 \times 1 \text{ cm}^2$		$0.75 \times 0.75 \text{ cm}^2$		$0.50 \times 0.50 \text{ cm}^2$		$0.25 \times 0.25 \text{ cm}^2$		
	Diode (%) [*]	MOSFET (%) [†]	Diode (%)	MOSFET (%)	Diode (%)	MOSFET (%)	Diode (%)	MOSFET (%)	Diode (%)	MOSFET (%)	
6 MV	0.5	0.8	-1.4	-4.8	-4.2	-5.1	-2.3	-6.1	2.3	-9.2	-7.8
	1.5	0.0	0.0	0.0	0.0	0.0	0.0	0.0	0.0	0.0	0.0
	5	1.4	2.9	-11.9	-12.5	-12.4	-11.8	-0.9	7.5	3.0	-21.6
	10	1.6	3.6	0.7	0.8	-0.4	3.9	-3.3	7.2	3.9	-12.6
	20	-0.2	-4.7	-0.4	-9.5	-2.2	-4.2	-6.8	-2.5	2.5	-9.7
15 MV	0.5	-8.8	-13.0	-11.7	-12.0	-13.2	-9.9	-16.4	-12.9	-20.6	15.2
	3	0.0	0.0	0.0	0.0	0.0	0.0	0.0	0.0	0.0	0.0
	5	-5.2	-6.4	0.9	-0.2	1.1	-1.0	0.6	-0.1	2.0	6.0
	10	-0.1	-2.9	0.8	1.1	1.1	1.7	-0.6	1.8	4.2	19.4
	20	-0.7	-8.5	-0.7	-4.8	1.5	0.0	-1.4	-6.4	5.9	22.5

^{*}Percentage differences between the PDD values measured by the diode detector (RAZOR detector) and those calculated by Eclipse.

[†]Percentage differences between the PDD values measured by the MOSFET detector and those calculated by Eclipse.

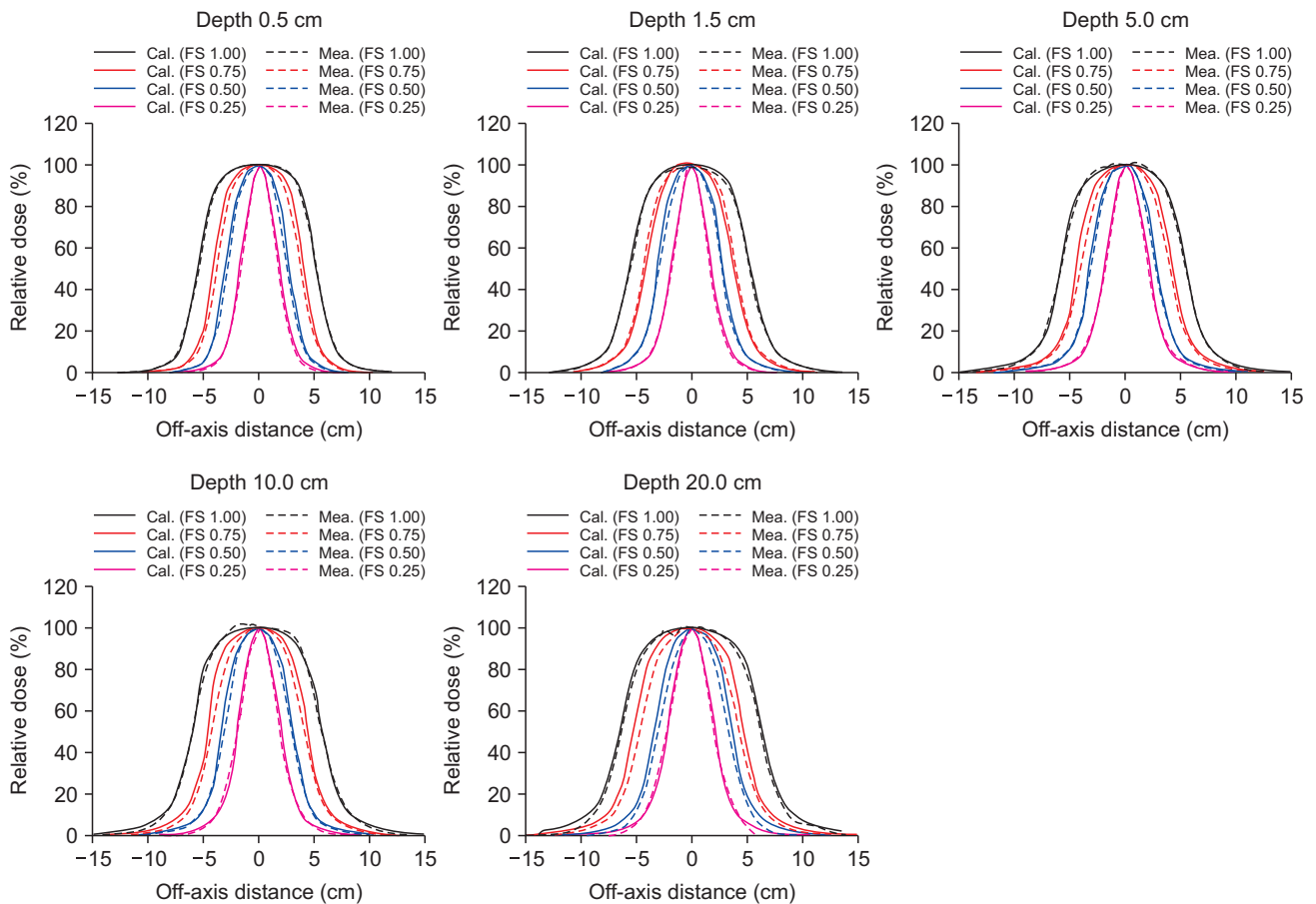


Fig. 3. Calculated and measured lateral profiles at various depths of 0.5 cm, 5 cm, 10 cm, 20 cm, and at the depth of the maximum dose (D_{max}) for the 6 MV photon beam for field sizes of $1 \times 1 \text{ cm}^2$, $0.75 \times 0.75 \text{ cm}^2$, $0.50 \times 0.50 \text{ cm}^2$, and $0.25 \times 0.25 \text{ cm}^2$. The value of D_{max} for 6 MV is 1.5 cm. The calculated and measured lateral profiles are plotted using solid and dashed lines, respectively.

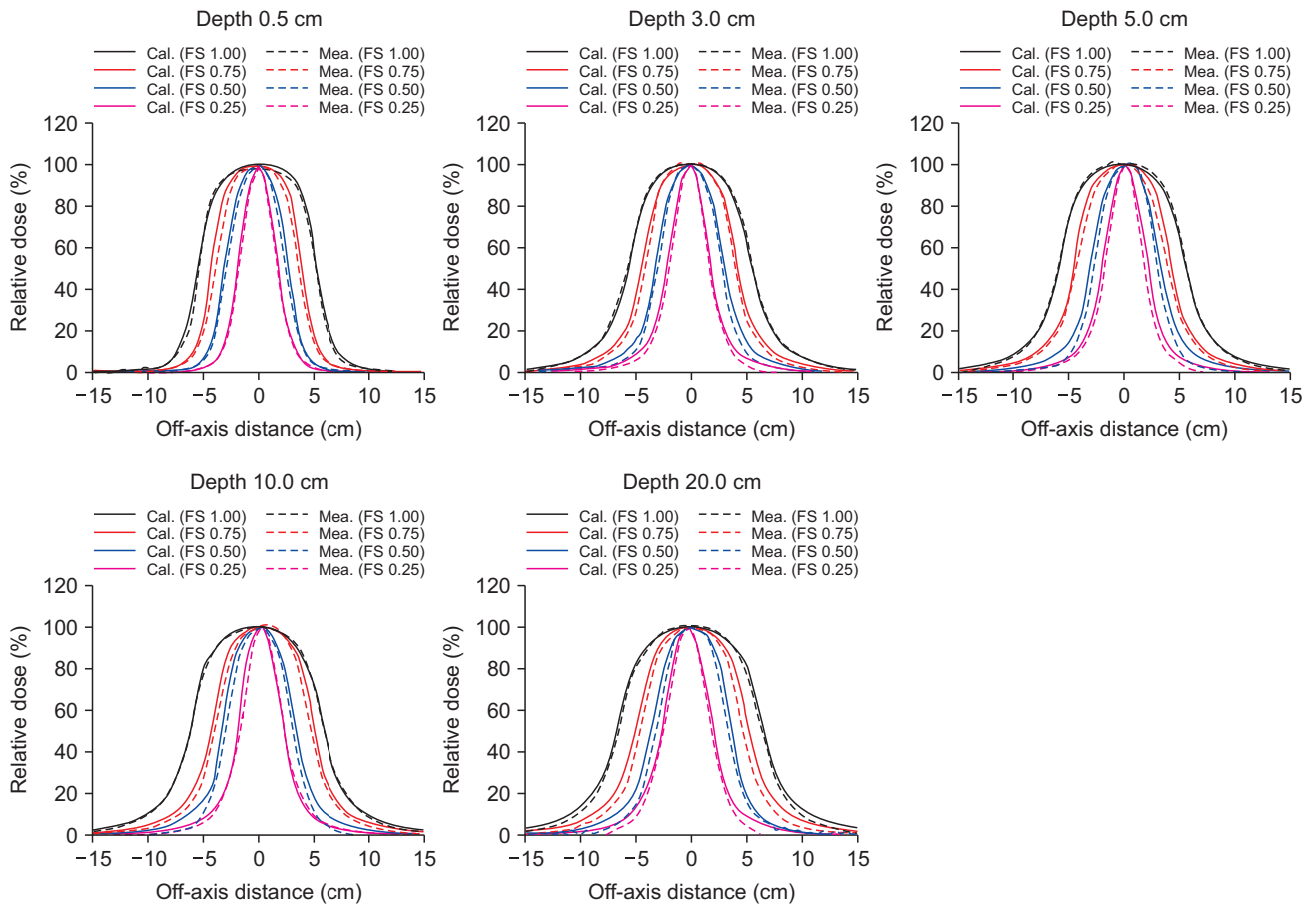


Fig. 4. Calculated and measured lateral profiles at various depths of 0.5 cm, 5 cm, 10 cm, 20 cm, and at a depth of maximum dose (D_{max}) for the 6 MV photon beam for the field sizes of $1 \times 1 \text{ cm}^2$, $0.75 \times 0.75 \text{ cm}^2$, $0.50 \times 0.50 \text{ cm}^2$, and $0.25 \times 0.25 \text{ cm}^2$. The value of D_{max} for 15 MV is 3 cm. The calculated and measured lateral profiles are plotted using solid and dashed lines, respectively.

Table 2. Values of absolute doses calculated from Eclipse and measured by MOSFET detectors for the photon beams of 6 MV and 15 MV at various depths equal to 0.5 cm, 5 cm, 10 cm, and 20 cm, and at the depth of the maximum dose (D_{max}) for field sizes equal to $10 \times 10 \text{ cm}^2$, $1 \times 1 \text{ cm}^2$, $0.75 \times 0.75 \text{ cm}^2$, $0.50 \times 0.50 \text{ cm}^2$, and $0.25 \times 0.25 \text{ cm}^2$. Percentage differences were calculated using the measured and calculated values. The D_{max} values for the photon beams of 6 MV and 15 MV are respectively equal to 1.5 cm and 3 cm.

Depth (cm)		Field size														
		$10 \times 10 \text{ cm}^2$			$1 \times 1 \text{ cm}^2$			$0.75 \times 0.75 \text{ cm}^2$			$0.50 \times 0.50 \text{ cm}^2$			$0.25 \times 0.25 \text{ cm}^2$		
		Cal.* (cGy)	Mea.† (cGy)	Diff.‡ (%)	Cal. (cGy)	Mea. (cGy)	Diff. (%)	Cal. (cGy)	Mea. (cGy)	Diff. (%)	Cal. (cGy)	Mea. (cGy)	Diff. (%)	Cal. (cGy)	Mea. (cGy)	Diff. (%)
6 MV	0.5	88.6	86.2	-2.7	98.9	94.3	-4.6	92.5	83.3	-9.9	84.7	71.3	-15.7	90.4	111.0	22.8
	1.5	100.0	98.7	-1.3	106.7	106.3	-0.4	95.4	88.0	-7.8	82.6	68.0	-17.6	86.4	115.0	33.1
	5	85.7	87.0	1.5	97.1	84.7	-12.8	86.5	70.3	-18.7	65.1	57.7	-11.5	68.0	71.0	4.4
	10	66.3	67.8	2.3	61.1	61.3	0.4	54.3	52.0	-4.2	46.8	41.3	-11.7	49.0	57.0	16.3
	20	38.6	36.3	-6.0	32.6	29.4	-9.8	28.8	25.5	-11.7	24.7	19.8	-19.7	25.8	31.0	20.2
15 MV	0.5	73.5	61.6	-16.2	105.95	93	-12.2	99.1	85.5	-13.7	90.45	76	-16.0	75.3	86.1	14.3
	3	99.4	95.8	-3.6	132.35	132	-0.3	111.7	107	-4.2	90.15	87	-3.5	71.1	70.6	-0.7
	5	98.9	89.2	-9.8	119.5	119	-0.4	100.7	95.5	-5.2	81.45	78.5	-3.6	64.5	67.9	5.3
	10	76.6	71.7	-6.4	93.25	94	0.8	78.55	76.5	-2.6	63.65	62.5	-1.8	50.6	60.0	18.6
	20	50.1	44.2	-11.8	57.95	55	-5.1	48.5	46.45	-4.2	90.45	76	-9.6	30.9	37.6	21.7

*Absolute doses calculated by Eclipse. †Absolute doses calculated with the use of MOSFET detectors. ‡Percentage differences between the absolute doses measured by the MOSFET detector and those calculated by Eclipse.

matched with those calculated by the Eclipse. At the depth of 20 cm, measured lateral profiles were underestimated in the shoulder of the profiles, compared with the calculated profiles.

2. Analyses of absolute doses

The absolute doses calculated from Eclipse and measured by MOSFET detectors and the percentage differences between them are shown in Table 2. At a depth equal to D_{\max} , there were good agreements between the calculations and measurements. The maximum percentage difference was 22.8% for the 6 MV photon beam with a field size of $0.25 \times 0.25 \text{ cm}^2$ and a depth of 0.5 cm. As the field sizes decreased, the percentage differences increased.

Discussion

To evaluate the performance of the diodes, MOSFET detectors and EBT3 films in small-field dosimetry, PDDs, and lateral profiles were measured by these detectors and absolute dosimetry was conducted with EBT3 films. Subsequently, we compared the calculations and measurements at various depths for field sizes of $1 \times 1 \text{ cm}^2$, $0.75 \times 0.75 \text{ cm}^2$, $0.50 \times 0.50 \text{ cm}^2$, and $0.25 \times 0.25 \text{ cm}^2$. Several studies have reported that there was an over-response of the diodes based on Monte Carlo simulations¹⁶⁻¹⁸⁾ or experimental determinations.^{15,19)} This over-response was mainly caused by the silicon chip that consisted of a higher density compared to water.⁹⁾ For this reason, correction factors for various types of diodes placed in a similar setup have been calculated and applied for various measurements.^{15,20,21)} With the exception of superficial depths (0.5 cm), most of the values measured by diodes were overestimated compared to those calculated by Eclipse, as shown in Table 1. For accurate dosimetry in small fields, the correction factors of the diodes should be considered.

At the depths of 0.5 cm and 20 cm, large percentage differences between the calculations and measurements of PDDs, lateral profiles, and absolute doses, were observed for both photon energies. It was demonstrated that large uncertainties occurred in the region before the build-up owing to a steep dose gradient and variations in the energy

spectrum in deeper depths that could make the measurements difficult.^{22,23)} However, the overall results elicited by diodes were better than those of MOSFET detectors because MOSFET detectors have high-angular dependencies and large active volumes that can often lead to uncertainties in dosimetry.²⁴⁾

As shown in Fig. 3 and 4, there is good agreement between the EBT3-measured and calculated lateral profiles in the high-dose region. This finding was consistent with the results of several prior studies.^{22,25)} Because an active volume of detectors is mainly an important factor for small-field measurements, superior spatial resolution for films is a favorable characteristic in small-field dosimetry.²⁶⁾ However, EBT3 films have a number of uncertainty from film position on the scanner, lack of uniformity in the scan area and a lack of uniformity of the active layer in the EBT3 films. Thus, correction factors should be considered in small-field dosimetry with the use of films to ensure for measurement stability.

Conclusion

In this study, we assessed the performance of various detectors, such as diodes, MOSFET detectors, and EBT3 films, in small-field dosimetry. There were good agreements between the calculations and measurements conducted by diodes and EBT films. Diode detectors and EBT3 films were found to be an appropriate option to the relative measurements of PDDs and lateral profiles, respectively.

Acknowledgements

This research was supported by Basic Science Research Program through the National Research Foundation of Korea (NRF) funded by the Ministry of Education (NRF-2017R1D1A1B03036093).

Conflicts of Interest

The authors have nothing to disclose.

Availability of Data and Materials

All relevant data are within the paper and its Supporting Information files.

References

- Ezzell GA, Galvin JM, Low D, et al. Guidance document on delivery, treatment planning, and clinical implementation of IMRT: report of the IMRT Subcommittee of the AAPM Radiation Therapy Committee. *Med phys.* 2003;30(8):2089-115.
- Zhang P, Happersett L, Hunt M, Jackson A, Zelefsky M, Mageras G. Volumetric modulated arc therapy: planning and evaluation for prostate cancer cases. *Int J Radiat Oncol Biol Phys.* 2010;76(5):1456-62.
- Evans JD, Hansen CC, Tollefson MK, Hallemeier CL. Stereotactic body radiation therapy for medically inoperable, clinically localized, urothelial carcinoma of the renal pelvis: A case report. *Adv Radia Oncol.* 2018;3(1):57-61.
- Alagar AG, Mani GK, Karunakaran K. Percentage depth dose calculation accuracy of model based algorithms in high energy photon small fields through heterogeneous media and comparison with plastic scintillator dosimetry. *J Appl Clin Med Phys.* 2016;17(1):132-42.
- Fogliata A, Cozzi L. Dose calculation algorithm accuracy for small fields in non-homogeneous media: The lung SBRT case. *Phys Med.* 2017;44:157-62.
- Adamczyk M, Fundowicz M. Stereotactic body radiation therapy for liver metastasis--case report and review of the literature. The role of patient preparation, treatment planning and its delivery. *J Cancer Res Ther.* 2014;10(3):519-25.
- Godson HF, Ravikumar M, Sathiyam S, Ganesh KM, Ponmalar YR, Varatharaj C. Analysis of small field percent depth dose and profiles: Comparison of measurements with various detectors and effects of detector orientation with different jaw settings. *J Med Phys.* 2016;41(1):12-20.
- Reggiori G, Mancosu P, Suchowerska N, et al. Characterization of a new unshielded diode for small field dosimetry under flattening filter free beams. *Phys Med.* 2016;32(2):408-13.
- Lechner W, Palmans H, Solkner L, Grochowska P, Georg D. Detector comparison for small field output factor measurements in flattening filter free photon beams. *Radiotherapy and oncology : Radiother Oncol.* 2013;109(3):356-60.
- Cranmer-Sargison G, Weston S, Evans JA, Sidhu NP, Thwaites DI. Implementing a newly proposed Monte Carlo based small field dosimetry formalism for a comprehensive set of diode detectors. *Med phys.* 2011;38(12):6592-602.
- Charles PH, Crowe SB, Kairn T, et al. Monte Carlo-based diode design for correction-less small field dosimetry. *Phys Med Biol.* 2013;58(13):4501-12.
- Amin MN, Heaton R, Norrlinger B, Islam MK. Small field electron beam dosimetry using MOSFET detector. *J Appl Clin Med Phys.* 2010;12(1):3267.
- Gonzalez-Lopez A, Vera-Sanchez JA, Lago-Martin JD. Small fields measurements with radiochromic films. *J Med Phys.* 2015;40(2):61-7.
- Morales JE, Hill R, Crowe SB, Kairn T, Trapp JV. A comparison of surface doses for very small field size x-ray beams: Monte Carlo calculations and radiochromic film measurements. *Australas Phys Eng Sci Med.* 2014;37(2):303-9.
- Ralston A, Liu P, Warrenner K, McKenzie D, Suchowerska N. Small field diode correction factors derived using an air core fibre optic scintillation dosimeter and EBT2 film. *Phys Med Biol.* 2012;57(9):2587-602.
- Scott AJ, Nahum AE, Fenwick JD. Using a Monte Carlo model to predict dosimetric properties of small radiotherapy photon fields. *Med phys.* 2008;35(10):4671-84.
- Scott AJ, Nahum AE, Fenwick JD. Monte Carlo modeling of small photon fields: quantifying the impact of focal spot size on source occlusion and output factors, and exploring miniphantom design for small-field measurements. *Med phys.* 2009;36(7):3132-44.
- Francescon P, Kilby W, Satariano N, Cora S. Monte Carlo simulated correction factors for machine specific reference field dose calibration and output factor measurement using fixed and iris collimators on the CyberKnife system. *Phys Med Biol.* 2012;57(12):3741-58.
- Pantelis E, Moutsatsos A, Zourari K, et al. On the output factor measurements of the CyberKnife iris collimator small fields: Experimental determination of the $k(Q(\text{clin}),Q(\text{msr})) (f(\text{clin}),f(\text{msr}))$ correction factors for microchamber and diode detectors. *Med phys.* 2012;39(8):

- 4875-85.
20. Ciancaglioni I, Marinelli M, Milani E, et al. Dosimetric characterization of a synthetic single crystal diamond detector in clinical radiation therapy small photon beams. *Med phys.* 2012;39(7):4493-501.
 21. Laub WU, Crilly R. Clinical radiation therapy measurements with a new commercial synthetic single crystal diamond detector. *J Appl Clin Med Phys.* 2014;15(6):4890.
 22. Massillon JLG, Cueva-Procel D, Diaz-Aguirre P, Rodriguez-Ponce M, Herrera-Martinez F. Dosimetry for small fields in stereotactic radiosurgery using gafchromic MD-V2-55 film, TLD-100 and alanine dosimeters. *PloS one.* 2013;8(5):e63418.
 23. Crop F, Reynaert N, Pittomvils G, et al. The influence of small field sizes, penumbra, spot size and measurement depth on perturbation factors for microionization chambers. *Phys Med Biol.* 2009;54(9):2951-69.
 24. Parwaie W, Refahi S, Ardekani MA, Farhood B. Different Dosimeters/Detectors Used in Small-Field Dosimetry: Pros and Cons. *J Med Signals Sens.* 2018;8(3):195-203.
 25. Novotny J, Jr., Bhatnagar JP, Quader MA, Bednarz G, Lunsford LD, Huq MS. Measurement of relative output factors for the 8 and 4 mm collimators of Leksell Gamma Knife Perfexion by film dosimetry. *Med phys.* 2009;36(5):1768-74.
 26. Qin Y, Gardner SJ, Kim J, et al. Technical Note: Evaluation of plastic scintillator detector for small field stereotactic patient-specific quality assurance. *Med phys.* 2017;44(10):5509-16.